

# Electric-Field Control of Spin-Orbit Torques in Perpendicularly Magnetized W/CoFeB/MgO Films

Mariia Filianina<sup>1,2</sup>, Jan-Philipp Hanke<sup>1,3</sup>, Kyujoon Lee<sup>1</sup>, Dong-Soo Han<sup>1,4</sup>, Samridh Jaiswal<sup>1,5</sup>, Adithya Rajan<sup>1</sup>, Gerhard Jakob<sup>1,2</sup>, Yuriy Mokrousov<sup>1,3</sup> and Mathias Kläui<sup>1,2,\*</sup>

<sup>1</sup>*Institute of Physics, Johannes Gutenberg University, 55099 Mainz, Germany*

<sup>2</sup>*Graduate School of Excellence Material Science in Mainz, 55099 Mainz, Germany*

<sup>3</sup>*Peter Grünberg Institut and Institute for Advanced Simulation, Forschungszentrum Jülich and JARA, 52425 Jülich, Germany*

<sup>4</sup>*Center for Spintronics, Korea Institute for Science and Technology, 02792 Seoul, Republic of Korea*

<sup>5</sup>*Singulus Technology AG, 63796 Kahl am Main, Germany*

(Received 13 January 2020; revised manuscript received 3 April 2020; accepted 29 April 2020)

Controlling magnetism by electric fields offers a highly attractive perspective for designing future generations of energy-efficient information technologies. Here, we demonstrate that the magnitude of current-induced spin-orbit torques in thin perpendicularly magnetized CoFeB films can be tuned and even increased by electric-field generated piezoelectric strain. Using theoretical calculations, we uncover that the subtle interplay of spin-orbit coupling, crystal symmetry, and orbital polarization is at the core of the observed strain dependence of spin-orbit torques. Our results open a path to integrating two energy efficient spin manipulation approaches, the electric-field-induced strain and the current-induced magnetization switching, thereby enabling novel device concepts.

DOI:

Controlling efficiently the magnetization of nanoscale devices is essential for many applications in spintronics, and is, thus, attracting significant attention in basic and applied science. In recent years, current-induced switching via spin-orbit torques (SOTs) [1] has emerged as one of the most promising approaches to realize scalable magnetoresistive random-access memories (MRAM). The SOT-induced switching is realized in a ferromagnet-heavy metal (FM-HM) bilayers, where the existence of sizable dampinglike  $\mathbf{T}^{\parallel} \propto \mathbf{m} \times (\mathbf{y} \times \mathbf{m})$  and fieldlike  $\mathbf{T}^{\perp} \propto \mathbf{m} \times \mathbf{y}$  components of the SOT due to the flow of an electrical current along the  $x$  direction was theoretically and experimentally studied [2–9]. These torques originate from the spin Hall effect in the bulk of the HM material [10] and the inverse spin galvanic effect at the FM-HM interface [11].

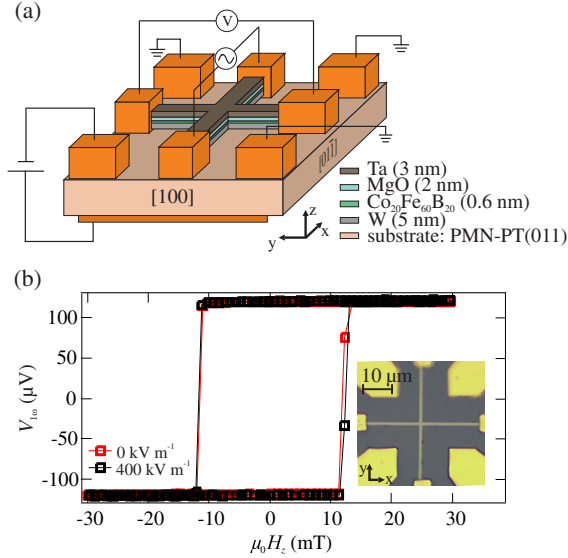
It was shown that the dampinglike torque term can be large enough to switch the magnetization direction at low current densities down to  $10^7$ – $10^8$  A cm<sup>-2</sup> [6,12], which makes them particularly attractive for device applications [13].

While sample parameters such as composition and layer thickness of FM-HM heterostructures can be adjusted to design the magnitude and the sign of SOTs, their “dynamical” control in a given system on-demand by external means is of great fundamental and technological interest. One of the energy-efficient tools for that is offered by the use of electric-field-induced mechanical strain [14]. Avoiding the need for electrical currents and, thus, eliminating the associated losses, strain is known to effectively tune magnetic properties such as magnetic anisotropy and, consequently, the magnetic domain structure and dynamics

of in-plane thin films [15–18]. Moreover, as strain can be applied locally, it provides a playground to develop and realize complex switching concepts in simplified device architectures.

While attempts were made to investigate the effect of strain on switching by spin torques [19–21], primarily the effect of strain on the anisotropy and the resulting impact on the switching was studied. Furthermore, these previous studies focused exclusively on systems with in-plane magnetic easy axis and experimental studies in perpendicularly magnetized multilayers are still elusive. However, in the light of the potential for technological applications, it is most desirable to optimize all magnetic parameters including the SOTs in ferromagnetic elements. In particular using systems with perpendicular magnetic anisotropy (PMA) is attractive as increased thermal stability, higher packing densities, and improved scaling behavior are intrinsic to PMA materials as compared to their in-plane magnetized counterparts [22,23].

In this work, we demonstrate electrically induced strain control of SOTs in perpendicularly magnetized W/CoFeB/MgO multilayers grown on a piezoelectric substrate. The SOTs are evaluated by magnetotransport and second-harmonic methods under in-plane strain of different character and magnitudes. We find that the strain, as modulated by the electric field applied across the piezoelectric substrate, leads to distinct responses of fieldlike and dampinglike torques, with a large change of the latter by a factor of 2. Based on the electronic structure of realistic heterostructures, we explain our experimental findings by theoretical *ab initio* calculations and reveal the microscopic



F1:1 FIG. 1. (a) Schematic of the Hall-cross device fabricated on top  
 F1:2 of the PMN-PT(011) substrate and the electrical contacts to the  
 F1:3 Hall bar as well as additional electrical contacts used for the  
 F1:4 application of the OOP electric field to generate strain. In this  
 F1:5 configuration the current flow ( $x$  axis) is along the  $[01\bar{1}]$  direction  
 F1:6 of the PMN-PT substrate, thus, in the text it is referred to as  
 F1:7 tensile strain configuration. For compressive strain, the current  
 F1:8 flow ( $x$  axis) is along the  $[100]$  direction. (b)  $1\omega$  Hall voltage  
 F1:9 hysteresis loop measured in the OOP direction at 0 (red), and  
 F1:10  $400 \text{ kV m}^{-1}$  (black) applied to the PMN-PT substrate using a  
 F1:11 current of  $0.33 \text{ mA}$ . The inset shows the optical microscope  
 F1:12 image of the Hall-cross structure used for the spin torque  
 F1:13 measurements.

81 origin of the observed strain effects on the magnetoelectric  
 82 coupling and the spin-orbit torques.

83 Figure 1(a) shows the schematic of the Hall-cross  
 84 device employed for the measurements of the dampinglike  
 85 (DL) and the fieldlike (FL) effective SOT fields in W(5 nm)/  
 86 CoFeB(0.6 nm)/MgO(2 nm)/Ta(3 nm) multilayer fabricated  
 87 on a  $[\text{Pb}(\text{Mg}_{0.33}\text{Nb}_{0.66}\text{O}_3)]_{0.68}\text{-}[\text{PbTiO}_3]_{0.32}$ (011) (PMN-PT)  
 88 substrate, employed to electrically generate mechanical strain  
 89 [24]. An optical microscope image of the Hall-cross device  
 90 used in the experiment is presented in the inset in Fig. 1(b)  
 91 and more details are provided in the Supplemental Material [24].

92 Uniaxial in-plane strain was generated by applying an  
 93 out-of-plane (OOP) dc electric field across the piezoelectric  
 94 PMN-PT(011) substrate. Generally, the piezoelectric strain  
 95 response to the applied electric field exhibits a hysteretic  
 96 behavior [38]. However, electric fields that exceed the  
 97 material-specific coercive field pole the substrate and lead  
 98 to a regime where the generated strain is characterized by  
 99 a linear response. The linear regime is maintained until the  
 100 substrate is poled in the other direction by application of  
 101 the electric fields larger than the opposite coercive field [38].  
 102 Therefore, before the first measurements, but after the  
 103 structuring process, we poled the PMN-PT substrate by  
 104 applying an electric field of  $+400 \text{ kV m}^{-1}$ . In the following,

105 we used the dc electric fields that allowed us to vary the strain  
 106 within the linear response regime [38], as this provides  
 107 reliable electrical control over the induced strain.

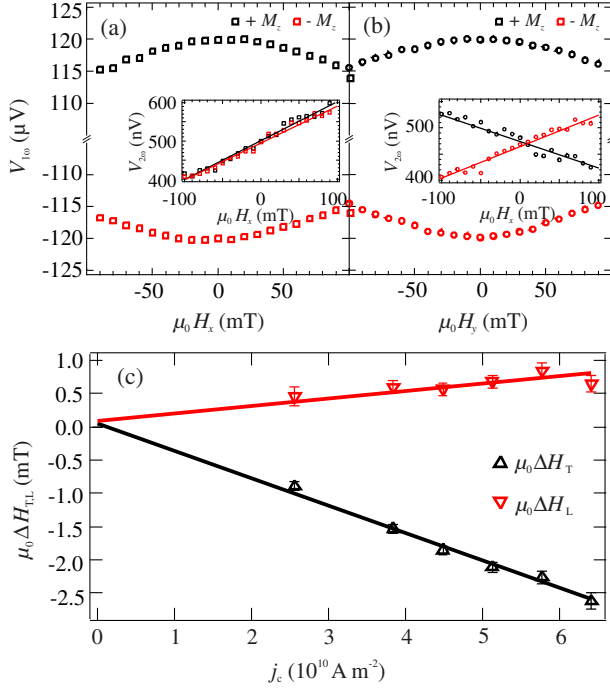
108 We also note that the Hall cross in Fig. 1(b) was  
 109 fabricated such that the arms were oriented along the  
 110  $[01\bar{1}]$  and  $[100]$  directions of the PMN-PT(011) substrate,  
 111 which correspond to the directions of tensile and compres-  
 112 sive strain, respectively, as set by the crystallographic  
 113 structure of the substrate [38]. The experimental results of  
 114 the SOTs obtained in the configuration with the current  
 115 ( $x$  axis) flowing along the  $[01\bar{1}]$  and  $[100]$  directions will be  
 116 referred to as modified by tensile and compressive strain,  
 117 respectively, [Fig. 1(a)]. We present the estimation of the  
 118 strain exerted on the Hall bar due to the electric field  
 119 applied between the bottom electrode and all top electrodes  
 120 in the Supplemental Material [24]. We also note that in the  
 121 configuration shown in Fig. 1(a) the Hall bar itself acts as a  
 122 top electrode, so that uniform strain can be expected.

123 First, we characterize the magnetic hysteresis of the  
 124 system at zero dc electric field. Figure 1(b) shows the  
 125 anomalous Hall voltage sweep with the OOP magnetic field  
 126 ( $\mu_0 H_z$ ) measured for W/CoFeB/MgO/Ta at  $0 \text{ kV m}^{-1}$   
 127 (red line), demonstrating the easy-axis switching typical  
 128 for W-based thin CoFeB stacks. [39,40] The OOP mag-  
 129 netization loop, measured at  $400 \text{ kV m}^{-1}$  (black line), is  
 130 overlaid on top of it and shows no sizable change due to the  
 131 generated strain indicating that the system has always a  
 132 dominating PMA. This is further supported by the mea-  
 133 surements probing the anisotropy changes induced by the  
 134 strain presented in the Supplemental Material [24].

135 The current-induced effective SOT fields were measured  
 136 using  $2\omega$  Hall measurements [41,42], as the high harmonic  
 137 technique provides robust determination of relative changes  
 138 of the SOTs [1] (see Supplemental Material [24] for more  
 139 details).

140 Figure 2 shows the representative in-plane field depend-  
 141 encies of the first ( $V_{1\omega}$ ) and the second ( $V_{2\omega}$ ) harmonics of  
 142 the Hall voltage when an ac current with the current density  
 143 of  $j_c = 3.8 \times 10^{10} \text{ A m}^{-2}$  was applied to the current line.  
 144 The dc poling voltage was set to zero, thus, no strain was  
 145 imposed on the Hall cross. The longitudinal [Fig. 2(a)] and  
 146 the transverse [Fig. 2(b)] field sweeps exhibit the expected  
 147 symmetries: for the longitudinal field, the slopes of  $V_{2\omega}$   
 148 versus the field are the same for both magnetization  
 149 directions along  $+z$  ( $+M_z$ ) or  $-z$  ( $-M_z$ ), whereas their  
 150 sign reverses for the transverse field sweep.

151 Using the procedure described in the Supplemental  
 152 Material [24] we analyze the transverse ( $\mu_0 \Delta H_T$ ) and the  
 153 longitudinal ( $\mu_0 \Delta H_L$ ) components of the SOT effective  
 154 field for both magnetization directions  $\pm M_z$  and plot the  
 155 average of these field components as a function of the  
 156 applied current density  $j_c$  in Fig. 2(c). The resulting linear  
 157 dependencies are fitted such that the slopes  $\mu_0 \Delta H_T / j_c$  and  
 158  $\mu_0 \Delta H_L / j_c$  determine the FL,  $\mu_0 H_{FL}^{\text{eff}}$ , and the DL,  
 159  $\mu_0 H_{DL}^{\text{eff}}$ , SOT effective fields, respectively. Similarly, the effective

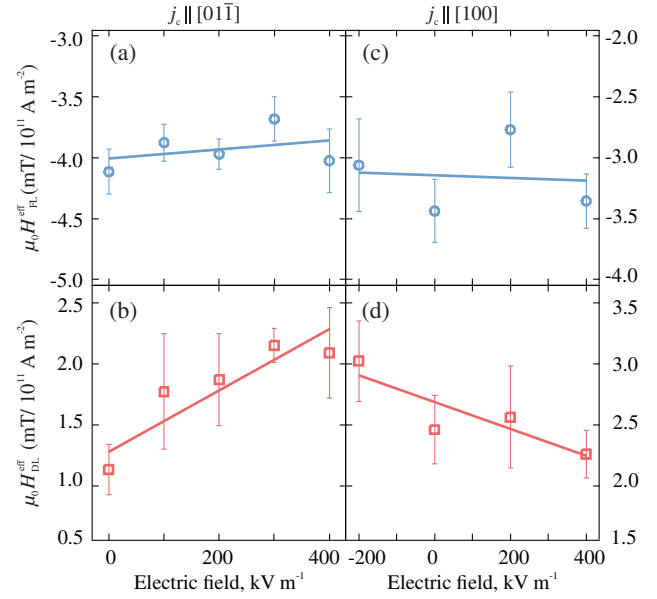


F2:1 FIG. 2. (a)  $V_{1\omega}$  and  $V_{2\omega}$  (inset) signals as a function of the in-  
 F2:2 plane field directed along the current flow. (b)  $V_{1\omega}$  and  $V_{2\omega}$  (inset)  
 F2:3 signals as a function of the in-plane field directed transverse to the  
 F2:4 current flow. The data were measured at the current density of  
 F2:5  $3.8 \times 10^{10} \text{ A m}^{-2}$ . Black and red symbols represent signals for  
 F2:6 the magnetization pointing along  $+z$  and  $-z$ , respectively. (c) The  
 F2:7 longitudinal ( $\mu_0 \Delta H_L$ ) and the transverse ( $\mu_0 \Delta H_T$ ) components of  
 F2:8 the SOT effective field plotted as a function of current density  $j_c$ .  
 F2:9 At each value of current density, the averaged values of the SOT  
 F2:10 effective field for  $+M_z$  and  $-M_z$  are shown.

160 fields were extracted for different dc electric fields applied  
 161 to the PMN-PT substrate to vary the magnitude of the  
 162 generated strain.

163 The electric-field dependent results are summarized in  
 164 Fig. 3. We find that the FL torque does not change  
 165 significantly for both tensile and compressive strains as  
 166 shown in Figs. 3(a) and 3(c). On the contrary, Fig. 3(b)  
 167 demonstrates that the tensile strain increases the DL torque  
 168 up to 2 times when  $400 \text{ kV m}^{-1}$  is applied, which corre-  
 169 sponds to ca. 0.03% strain [24,38]. On the other hand, when  
 170 the current is flowing along the compressive strain direction,  
 171 the magnitude of the DL torque decreases with increasing  
 172 strain. Thus, we find experimentally that the magnitude of  
 173 the DL torque increases (decreases) upon the application of  
 174 electrically induced tensile (compressive) strain.

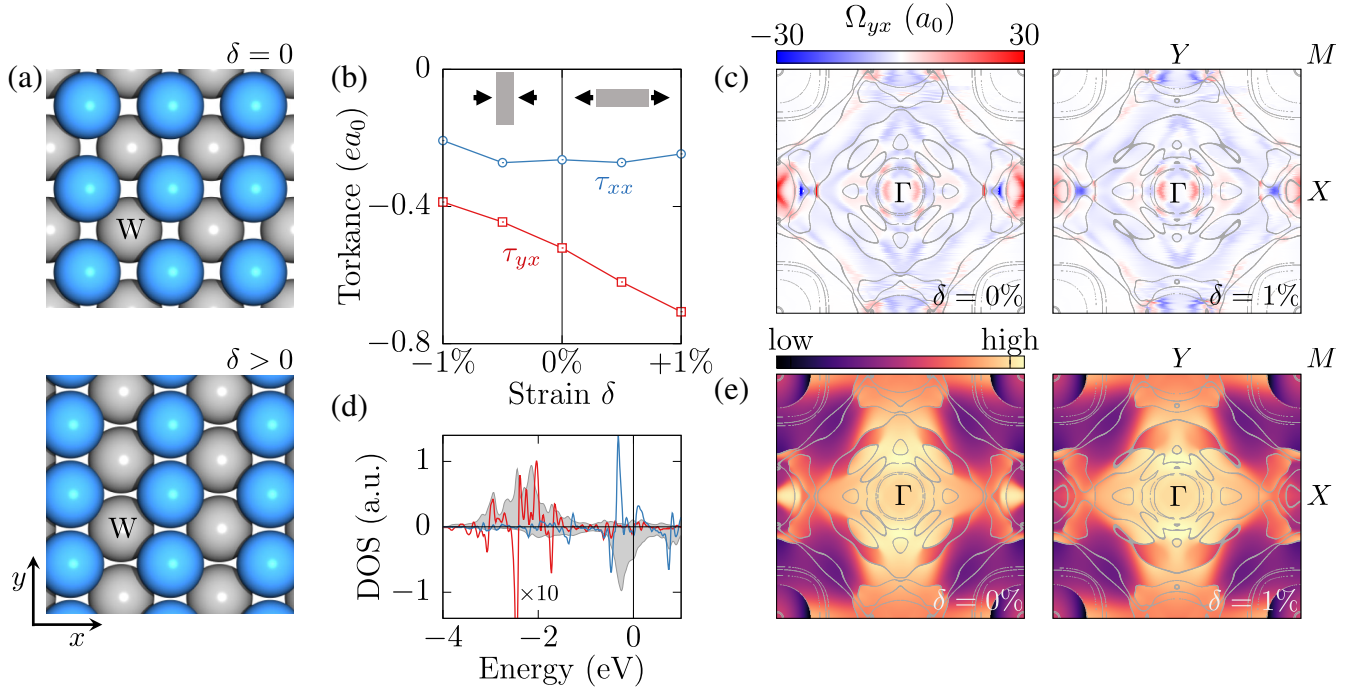
175 In order to understand the microscopic origin of the  
 176 experimentally observed strain dependence of FL and DL  
 177 SOTs, we perform density functional theory calculations of  
 178 the electronic structure of  $\text{Fe}_{1-x}\text{Co}_x/\text{W}(001)$ , which con-  
 179 sists of a perpendicularly magnetized monolayer and non-  
 180 magnetic underlayers (see Supplemental Material [24]).  
 181 As illustrated in Fig. 4(a), we expand or contract the crystal  
 182 structure while keeping the in-plane area of the unit cell



F3:1 (a) FL and (b) DL SOT effective fields as a function of  
 F3:2 the electric field applied across the PMN-PT(011) for the current  
 F3:3 flowing along the tensile ( $[01\bar{1}]$ ) strain direction. (c) FL and  
 F3:4 (d) DL SOT effective fields as a function of the electric field  
 F3:5 applied for the current flowing along the compressive ( $[100]$ )  
 F3:6 strain direction. The solid lines represent the linear fit of the data  
 F3:7 to guide the eye.

183 constant to account for the effect of uniaxial strain. This  
 184 strain can be quantified by the ratio  $\delta = (a'_j - a_j)/a_j$ ,  
 185 where  $a_j$  and  $a'_j$  denote the lattice constant along the  $j$ th  
 186 in-plane direction in the relaxed and distorted case,  
 187 respectively. As a consequence, any finite strain reduces  
 188 the original  $C_{4v}$  crystal symmetry to  $C_{2v}$ , see Fig. 4(a).  
 189 We employ a Kubo formalism [43] to represent the SOT  
 190  $T_i = \tau_{ij} E_j$  acting on the magnetization as the linear  
 191 response to the applied electric field  $E_j$ , mediated by the  
 192 torkance  $\tau_{ij}$ . Owing to the mirror symmetries of the strained  
 193 films with OOP magnetization, the torkances  $\tau_{xx}$  and  $\tau_{yy}$   
 194 characterize FL SOTs rooted in the electronic structure at  
 195 the Fermi surface, whereas  $\tau_{xy}$  and  $\tau_{yx}$  correspond to DL  
 196 torques, to which also electrons of the Fermi sea contribute.  
 197 In order to model additionally disorder and temperature  
 198 effects, we evaluate these response coefficients using a  
 199 constant broadening  $\Gamma = 25 \text{ meV}$  of the first-principles  
 200 energy bands [43]. In the following,  $\delta$  refers to the strain  
 201 along the orientation of the applied electric field, which  
 202 points into the  $x$  direction.

203 Based on our electronic-structure calculations, we obtain  
 204 the  $\delta$  dependence of the SOTs shown in Fig. 4(b), which  
 205 reveals similar qualitative trends as found in the experi-  
 206 ment. Since FL and DL SOTs originate from different  
 207 electronic states, they generally follow distinct dependen-  
 208 cies on structural details. Specifically, while the FL term  $\tau_{xx}$   
 209 is hardly affected if  $\delta$  is varied, we predict that the  
 210 magnitude of the DL torque  $\tau_{xy}$  increases (decreases)



F4:1 FIG. 4. (a) The uniaxial strain  $\delta$  modifies the equilibrium crystal structure of the  $\text{Fe}_{0.7}\text{Co}_{0.3}/\text{W}(001)$  film, and reduces the symmetry  
 F4:2 from  $C_{4v}$  to  $C_{2v}$ . (b) Dependence of FL (blue) and DL (red) torques on strain along the direction of the electric field, where a constant  
 F4:3 broadening of the energy bands by 25 meV is used. (c) Microscopic contribution of all occupied bands to the DL SOT in relaxed and  
 F4:4 strained crystal structure. Gray lines indicate the Fermi surface. (d) As compared to the behavior without strain (gray), the density of  $d_{yz}$   
 F4:5 states in the magnetic layer changes for majority (red) and minority (blue) spin channels owing to tensile strain of  $\delta = 1\%$ . The red and  
 F4:6 blue curves, showing the difference with respect to the unstrained case, are scaled by a factor of 10. (e) Momentum-space distribution of  
 F4:7 the  $d_{yz}$  polarization of all occupied majority states in the magnetic layer of the relaxed and strained system.

211 linearly with respect to tensile (compressive) strain. For  
 212 instance, expanding the lattice by 1% along the electric-  
 213 field direction drastically enhances the DL torque by  
 214 about 35%. To elucidate this remarkable behavior, we  
 215 compare in Fig. 4(c) the momentum-space distribution of  
 216 the microscopic contributions to the DL SOT for relaxed  
 217 and strained films. In contrast to the occupied states around  
 218 the  $M$  point that are barely important, electronic states near  
 219 the high-symmetry points  $\Gamma$ ,  $X$ , and  $Y$  constitute the major  
 220 source of the DL torque. In particular, tensile strain  
 221 promotes strong negative contributions around  $X$  and  $Y$   
 222 [see Fig. 4(c)], leading to an overall increase in the  
 223 magnitude of  $\tau_{yx}$  as depicted in Fig. 4(b).

224 To further associate our findings with the underlying  
 225 electronic structure, we turn to the orbital polarization of  
 226 the states in the magnetic layer, the physics of which is  
 227 dominated by  $d$  electrons. Whereas the behavior of  $d_{xy}$ ,  
 228  $d_{x^2-y^2}$ , and  $d_{z^2}$  is independent of the sign of the applied  
 229 strain  $\delta$ , the states of  $d_{yz}$  and  $d_{zx}$  character transform  
 230 manifestly differently with respect to tensile or compressive  
 231 strain. Remarkably, the latter orbitals also mediate the  
 232 hybridization with the heavy-metal substrate, which  
 233 implies that their dependence on structural details offers  
 234 additional microscopic insights into the SOTs in the studied  
 235 thin films. As an example, we consider in Fig. 4(d) the

236 strain-induced change of the density of  $d_{yz}$  states in the  
 237 magnetic layer as compared to the case with fourfold  
 238 rotational symmetry. While the density of minority-spin  
 239 states at the Fermi level is hardly affected by tensile strain,  
 240 the majority-spin states are redistributed rather strongly.  
 241 As revealed by the momentum-resolved orbital polarization  
 242 in Fig. 4(e), microscopically, this effect stems from  
 243 pronounced  $\delta$ -driven variations of the  $d_{yz}$  polarization  
 244 around the  $X$  point, which correlates with the presented  
 245 changes of the DL torque, Fig. 4(c).

246 As the system considered in this work has a relatively  
 247 strong PMA, the static magnetic properties of the CoFeB  
 248 film as visible from the hysteresis loop [Fig. 1(b)] did not  
 249 show any significant change with the applied strain. Prior  
 250 work has focused on systems where the dominating effect  
 251 of the strain was a change of the anisotropy [19–21],  
 252 but here we have strong PMA and probe the change of the  
 253 SOTs as the main factor. The sizable change in the torques  
 254 found can be explained by our theoretical calculations.

255 Using our microscopic insights obtained from the  
 256 electronic structure calculations, we uncovered that the  
 257 distinct nature of the experimentally observed trends for  
 258 FL and DL torques roots in unique changes of the orbital  
 259 polarization of the electronic states due to distortions of  
 260 the lattice. Beyond revealing the key role of hybridized

261 states at the FM-HM interface, our results suggest a clear  
 262 scheme for generally engineering spin-orbit phenomena.  
 263 Utilizing the complex interplay of spin and orbital magnet-  
 264 ism, spin-orbit coupling, and symmetry, we can tailor the  
 265 magnitude of SOTs in multilayer devices by designing the  
 266 orbital polarization of the states near the Fermi energy by  
 267 strain.

268 Importantly, our work opens up a route for shaping  
 269 fundamental spin-orbitronic concepts into competitive  
 270 technologies by dynamically tuning the SOTs in perpen-  
 271 dicularly magnetized multilayer systems by means of  
 272 electrically controlled strain. For example, as the strain  
 273 can be generated locally and imposed on selected parts of  
 274 the switching area, one can tune the current density such  
 275 that the DL torque is large enough to switch the magneti-  
 276 zation direction in these parts, while it is too small to switch  
 277 the unstrained parts. In this case it would be possible to  
 278 switch only selected parts of the area in one run with the  
 279 given current density. The selected parts can then be altered  
 280 on demand by utilizing a different configuration of the  
 281 electric fields, which allows for an additional level of  
 282 control. Thus, by designing particular strain patterns of the  
 283 switching area by electric fields, an energy efficient  
 284 multilevel memory cell capability can be realized, which  
 285 is practically important, e.g., for the emerging field of  
 286 neuromorphic computing [44].

287 In addition, we anticipate that strain will not only alter the  
 288 dynamical properties of topological spin textures but could  
 289 also modify the Dzyaloshinskii-Moriya interaction [45,46]  
 290 that may stabilize two-dimensional magnetic solitons. As a  
 291 consequence, strain offers an efficient means to control the  
 292 shape and nature of chiral spin structures such as skyrmions  
 293 [47] and antiskyrmions, which are perceived to hold bright  
 294 prospects for innovative information processing.

295 In conclusion, we studied the strain response of current-  
 296 induced SOTs in perpendicularly magnetized W/CoFeB/  
 297 MgO multilayers grown on a piezoelectric substrate.  
 298 The SOTs are evaluated by magnetotransport and sec-  
 299 ond-harmonic methods under in-plane strains of different  
 300 character and magnitude. We find that the strain leads to  
 301 distinctly different changes of FL and DL torques, with the  
 302 latter enhanced by roughly a factor of two if a tensile strain  
 303 is applied parallel to the current flow. Our experimental  
 304 results are in qualitative agreement with *ab initio* calcu-  
 305 lations that uncover the microscopic origin of the observed  
 306 strain effects on SOTs. We reveal that the character of strain  
 307 imprints on the orbital polarization of the electronic states  
 308 in the ferromagnet, which reflects directly the hybridization  
 309 with the HM underlayer. This manifests in a sizable variation  
 310 of the magnitude of the DL torque while the FL torque  
 311 remains mostly unaffected. The demonstrated possibility to  
 312 tune the SOTs by means of electric-field-induced strain paves  
 313 a novel path towards to the energy efficient dynamical control  
 314 of the current-driven SOT-switching necessary to enable  
 315 future spintronics applications.

The work was financially supported by the Deutsche 316  
 Forschungsgemeinschaft (DFG, German Research 317  
 Foundation) in particular by Grant No. KL1811/18 318  
 (318612841) and the Graduate School of Excellence 319  
 “Materials Science in Mainz” (DFG/GSC266). Y.M. 320  
 acknowledges support by the DFG through the Priority 321  
 Programme SPP 2137, and additional support was provided 322  
 by the Collaborative Research Center SFB/TRR173 323  
 (Projects No. A01—290396061/TRR173, A11—268565 324  
 370/TRR173 and B02—290319996/TRR173). A. R., G. J., 325  
 and M. K. acknowledge funding from the European 326  
 Union’s Framework Programme for Research and 327  
 Innovation Horizon 2020 (2014-2020) under the Marie 328  
 Skłodowska-Curie Grant Agreement No. 860060 (ITN 329  
 MagnEFi). D.-S.H. acknowledges funding from the 330  
 Korea Institute of Science and Technology (KIST) institu- 331  
 tional program (No. 2E30600) and the National Research 332  
 Council of Science & Technology (NST) grant (No. CAP- 333  
 16-01-KIST) funded by the Korea government (Ministry of 334  
 Science and ICT). J. H. and Y. M. also gratefully acknowl- 335  
 edge the Jülich Supercomputing Centre and RWTH 336  
 Aachen University for providing computational resources 337  
 under project jiff40. 338

\*Klaeui@uni-mainz.de

- 341  
 342  
 343  
 344  
 345  
 346  
 347  
 348  
 349  
 350  
 351  
 352  
 353  
 354  
 355  
 356  
 357  
 358  
 359  
 360  
 361  
 362  
 363  
 364  
 365  
 366  
 367  
 368  
 369  
 370  
 371  
 372  
 373  
 374
- [1] A. Manchon, J. Železný, I. M. Miron, T. Jungwirth, J. Sinova, A. Thiaville, K. Garello, and P. Gambardella, *Rev. Mod. Phys.* **91**, 035004 (2019).
  - [2] A. Manchon and S. Zhang, *Phys. Rev. B* **78**, 212405 (2008).
  - [3] I. M. Miron, G. Gaudin, S. Auffret, B. Rodmacq, A. Schuhl, S. Pizzini, J. Vogel, and P. Gambardella, *Nat. Mater.* **9**, 230 (2010).
  - [4] J. Kim, J. Sinha, M. Hayashi, M. Yamanouchi, S. Fukami, T. Suzuki, S. Mitani, and H. Ohno, *Nat. Mater.* **12**, 240 (2013).
  - [5] K. Garello, I. M. Miron, C. O. Avci, F. Freimuth, Y. Mokrousov, S. Blügel, S. Auffret, O. Boulle, G. Gaudin, and P. Gambardella, *Nat. Nanotechnol.* **8**, 587 (2013).
  - [6] L. Liu, C.-F. Pai, Y. Li, H. W. Tseng, D. C. Ralph, and R. A. Buhrman, *Science* **336**, 555 (2012).
  - [7] T. Schulz, K. Lee, B. Krüger, R. Lo Conte, G. V. Karnad, K. Garcia, L. Vila, B. Ocker, D. Ravelosona, and M. Kläui, *Phys. Rev. B* **95**, 224409 (2017).
  - [8] T. Schulz, O. Alejos, E. Martinez, K. M. D. Hals, K. Garcia, L. Vila, K. Lee, R. Lo Conte, G. V. Karnad, S. Moretti *et al.*, *Appl. Phys. Lett.* **107**, 122405 (2015).
  - [9] R. Lo Conte, A. Hrabec, A. P. Mihai, T. Schulz, S.-J. Noh, C. H. Marrows, T. A. Moore, and M. Kläui, *Appl. Phys. Lett.* **105**, 122404 (2014).
  - [10] J. Sinova, S. O. Valenzuela, J. Wunderlich, C. H. Back, and T. Jungwirth, *Rev. Mod. Phys.* **87**, 1213 (2015).
  - [11] V. V. Bel’kov and S. D. Ganichev, *Semicond. Sci. Technol.* **23**, 114003 (2008).
  - [12] I. M. Miron, K. Garello, G. Gaudin, P.-J. Zermatten, M. V. Costache, S. Auffret, S. Bandiera, B. Rodmacq, A. Schuhl, and P. Gambardella, *Nature (London)* **476**, 189 (2011).
  - [13] G. Prenat, K. Jabeur, P. Vanhauwaert, G. D. Pendina, F. Oboril, R. Bishnoi, M. Ebrahimi, N. Lamard, O. Boulle, and

- 375 K. Garello, *IEEE Trans. Multi-Scale Comput. Syst.* **2**, 49  
376 (2016).
- 377 [14] J. Wang, *Annu. Rev. Mater. Res.* **49**, 361 (2019).
- 378 [15] H. Sohn, M. E. Nowakowski, C.-y. Liang, J. L. Hockel, K.  
379 Wetzlar, S. Keller, B. M. McLellan, M. A. Marcus, A.  
380 Doran, and A. Young, *ACS Nano* **9**, 4814 (2015).
- 381 [16] S. Finizio, M. Foerster, M. Buzzi, B. Krüger, M. Jourdan,  
382 C. A. F. Vaz, J. Hockel, T. Miyawaki, A. Tkach, S. Valencia,  
383 F. Kronast, G. P. Carman, F. Nolting, and M. Kläui, *Phys.*  
384 *Rev. Applied* **1**, 021001 (2014).
- 385 [17] M. Filianina, L. Baldrati, T. Hajiri, K. Litzius, M. Foerster,  
386 L. Aballe, and M. Kläui, *Appl. Phys. Lett.* **115**, 062404  
387 (2019).
- 388 [18] M. Foerster, F. Maciá, N. Statuto, S. Finizio, A. Hernández-  
389 Mínguez, S. Lendínez, P. Santos, J. Fontcuberta, and J. M.  
390 Hernández, *Nat. Commun.* **8**, 407 (2017).
- 391 [19] Q. Wang, J. Domann, G. Yu, A. Barra, K. L. Wang, and G. P.  
392 Carman, *Phys. Rev. Applied* **10**, 034052 (2018).
- 393 [20] H. B. Huang, C. P. Zhao, and X. Q. Ma, *Adv. Condens.*  
394 *Matter Phys.* **2016**, 1 (2016).
- 395 [21] T. Nan, J.-M. Hu, M. Dai, S. Emori, X. Wang, Z. Hu, A.  
396 Matyushov, L.-Q. Chen, and N. Sun, *Adv. Funct. Mater.* **29**,  
397 1806371 (2019).
- 398 [22] N. Nishimura, T. Hirai, A. Koganei, T. Ikeda, K. Okano, Y.  
399 Sekiguchi, and Y. Osada, *J. Appl. Phys.* **91**, 5246 (2002).
- 400 [23] S. Ikeda, K. Miura, H. Yamamoto, K. Mizunuma, H. D.  
401 Gan, M. Endo, S. Kanai, J. Hayakawa, F. Matsukura, and H.  
402 Ohno, *Nat. Mater.* **9**, 721 (2010).
- 403 [24] See Supplemental Material at [http://link.aps.org/  
404 supplemental/10.1103/PhysRevLett.000.000000](http://link.aps.org/supplemental/10.1103/PhysRevLett.000.000000) for details  
405 of sample fabrication and the experimental and computa-  
406 tional methods as well as for the generated strain estimation  
407 and the anisotropy measurements, which includes Refs. [25–  
408 37].
- 409 [25] See <https://www.mtixtl.com>.
- 410 [26] S. Cho and B.-G. Park, *Curr. Appl. Phys.* **15**, 902 (2015).
- 411 [27] See <http://www.flapw.de>.
- 412 [28] J. P. Perdew, K. Burke, and M. Ernzerhof, *Phys. Rev. Lett.*  
413 **77**, 3865 (1996).
- [29] P. Ferriani, S. Heinze, G. Bihlmayer, and S. Blügel, *Phys.*  
414 *Rev. B* **72**, 024452 (2005). 415
- [30] L. Bellaïche and D. Vanderbilt, *Phys. Rev. B* **61**, 7877  
416 (2000). 417
- [31] J.-P. Hanke, F. Freimuth, S. Blügel, and Y. Mokrousov,  
418 *Phys. Rev. B* **91**, 184413 (2015). 419
- [32] J.-P. Hanke, F. Freimuth, S. Blügel, and Y. Mokrousov, *J.*  
420 *Phys. Soc. Jpn.* **87**, 041010 (2018). 421
- [33] N. Lobontiu, *System Dynamics for Engineering Students*  
422 (Elsevier, Boston, 2010), [https://doi.org/10.1016/C2011-0-  
423 05346-2](https://doi.org/10.1016/C2011-0-05346-2). 424
- [34] G. C. Kuczynski, *Phys. Rev.* **94**, 61 (1954). 425
- [35] P. Shepley, A. Rushforth, M. Wang, G. Burnell, and T. A.  
426 Moore, *Sci. Rep.* **5**, 7921 (2015). 427
- [36] See <http://www.innoviamaterials.com/about/?121.html>. 428
- [37] K.-W. Moon, J.-C. Lee, S.-B. Choe, and K.-H. Shin, *Rev.*  
429 *Sci. Instrum.* **80**, 113904 (2009). 430
- [38] T. Wu, P. Zhao, M. Bao, A. Bur, J. L. Hockel, K. Wong,  
431 K. P. Mohanchandra, C. S. Lynch, and G. P. Carman, *J.*  
432 *Appl. Phys.* **109**, 124101 (2011). 433
- [39] S. Jaiswal, K. Litzius, I. Lemesh, F. Büttner, S. Finizio, J.  
434 Raabe, M. Weigand, K. Lee, J. Lan, B. Ocker *et al.*, *Appl.*  
435 *Phys. Lett.* **111**, 022409 (2017). 436
- [40] Y. Takeuchi, C. Zhang, A. Okada, H. Sato, S. Fukami, and  
437 H. Ohno, *Appl. Phys. Lett.* **112**, 192408 (2018). 438
- [41] M. Hayashi, J. Kim, M. Yamanouchi, and H. Ohno, *Phys.*  
439 *Rev. B* **89**, 144425 (2014). 440
- [42] U. H. Pi, K. Won Kim, J. Y. Bae, S. C. Lee, Y. J. Cho,  
441 K. S. Kim, and S. Seo, *Appl. Phys. Lett.* **97**, 162507  
442 (2010). 443
- [43] F. Freimuth, S. Blügel, and Y. Mokrousov, *Phys. Rev. B* **90**,  
444 174423 (2014). 445
- [44] N. K. Upadhyay, H. Jiang, Z. Wang, S. Asapu, Q. Xia, and  
446 J. J. Yang, *Adv. Mater. Technol.* **4**, 1800589 (2019). 447
- [45] T. Moriya, *Phys. Rev.* **120**, 91 (1960). 448
- [46] I. Dzyaloshinsky, *J. Phys. Chem. Solids* **4**, 241 (1958). **2** 449
- [47] K. Shibata, J. Iwasaki, N. Kanazawa, S. Aizawa, T.  
450 Tanigaki, M. Shirai, T. Nakajima, M. Kubota, M. Kawasaki,  
451 H. S. Park *et al.*, *Nat. Nanotechnol.* **10**, 589 (2015). **3** 452  
453